Equilibrium model prediction for the scatter in the star-forming main sequence

Monthly Notices
of the
ROYAL ASTRONOMICAL SOCIETY

MNRAS **464,** 2766–2776 (2017)
Advance Access publication 2016 October 4

doi:10.1093/mnras/stw2527

Equilibrium model prediction for the scatter in the star-forming main sequence

Sourav Mitra,[1]★ Romeel Davé,[1,2,3] Vimal Simha[1] and Kristian Finlator[4]

[1]*University of the Western Cape, Bellville, Cape Town 7535, South Africa*
[2]*South African Astronomical Observatories, Observatory, Cape Town 7925, South Africa*
[3]*African Institute for Mathematical Sciences, Muizenberg, Cape Town 7945, South Africa*
[4]*New Mexico State University, Las Cruces, NM 88003-8001, USA*

Accepted 2016 October 3. Received 2016 September 22; in original form 2016 June 23; Editorial Decision 2016 September 30

ABSTRACT

The analytic 'equilibrium model' for galaxy evolution using a mass balance equation is able to reproduce mean observed galaxy scaling relations between stellar mass, halo mass, star formation rate (SFR), and metallicity across the majority of cosmic time with a small number of parameters related to feedback. Here, we aim to test this data-constrained model to quantify deviations from the mean relation between stellar mass and SFR, i.e. the star-forming galaxy main sequence (MS). We implement fluctuation in halo accretion rates parametrized from merger-based simulations, and quantify the intrinsic scatter introduced into the MS under the assumption that fluctuations in star formation follow baryonic inflow fluctuations. We predict the 1σ MS scatter to be $\sim$0.2–0.25 dex over the stellar mass range 10^8–10^{11} $M_\odot$ and a redshift range $0.5 \lesssim z \lesssim 3$ for SFRs averaged over 100 Myr. The scatter increases modestly at $z \gtrsim 3$, as well as by averaging over shorter time-scales. The contribution from merger-induced star formation is generally small, around 5 per cent today and 10–15 per cent during the peak epoch of cosmic star formation. These results are generally consistent with available observations, suggesting that deviations from the MS primarily reflect stochasticity in the inflow rate owing to halo mergers.

Key words: galaxies: abundances – galaxies: evolution – galaxies: formation – galaxies: luminosity function, mass function.

1 INTRODUCTION

Over the past few years, advances in large multiwavelength galaxy surveys have considerably increased our knowledge of galaxy evolution. In particular, such surveys have served to greatly constrain the scaling relations between global galaxy properties, which place constraints on the nature of galaxy growth. As observational uncertainties, both statistical and systematic, are lowered, key galaxy scaling relations have been shown to be quite tight, such as the relationship between stellar mass and gas-phase metallicity that shows a scatter of $\sim$0.1 dex or less (Tremonti et al. 2004). These scaling relations suggest an underlying simplicity involved in the various complex processes of galaxy evolution.

A particularly well-investigated scaling relation is that between the star formation rate (SFR) and stellar mass (M_*) in star-forming galaxies (SFGs), colloquially known as the SFG 'main sequence' (MS). The MS extends over several orders of magnitudes in M_* and out to high redshifts, with a modest scatter of $\sim$0.3 dex which includes both intrinsic scatter and measurement uncertainties. The existence of such tight scatter at all observed epochs suggests that most galaxies assembled their stellar mass fairly steadily rather than predominantly in starburst episodes, implying that mergers have a sub-dominant contribution to the global star formation history (SFH; Rodighiero et al. 2011; Sargent et al. 2012; Schreiber et al. 2015).

Concurrently, cosmological simulations highlighted the fact that the inflow of gas fuelling star formation into galaxies enters predominantly in smooth, cold accretion (Kereš et al. 2005; Dekel et al. 2009). However, it has long been recognized that unabated accretion would result in galaxies far too large compared to observations (White & Frenk 1991; Balogh et al. 2001), and solving this so-called 'overcooling problem' requires strong feedback to suppress star formation. The now-ubiquitous observations of galactic outflows in SFGs over much of cosmic time (Martin 2005; Weiner et al. 2009; Steidel et al. 2010; Rubin et al. 2014) suggest that such outflows are the primary mechanism for self-regulation in SFGs, by ejecting copious amounts of gas from galaxies that would otherwise form into stars. Simulations now routinely include such outflow processes in order to achieve good agreement with basic galaxy demographics (Di Cintio et al. 2014; Genel et al. 2014; Muratov et al. 2015; Schaye et al. 2015; Somerville & Davé 2015;

★ E-mail: hisourav@gmail.com

Christensen et al. 2016; Davé, Thompson & Hopkins 2016; Wetzel et al. 2016). Furthermore, models argue that the return of some outflow material, often called 'wind recycling', is also an important component of inflow required to match galaxy properties (e.g. Oppenheimer et al. 2010; Henriques et al. 2013). Thus it appears that, within the well-constrained growth of large-scale structure, the *baryon cycling* processes of inflows, outflows, and wind recycling govern the growth of galaxies across cosmic time.

While the physical mechanisms and dynamics require complex cosmologically based simulations to fully describe, it is possible to obtain intuitive insights and robust constraints on baryon cycling processes using a simple analytic framework. The essential equation balances the gas inflow rate into the interstellar medium (ISM) of galaxies, versus the sum of the mass outflow rate and SFR, as well as fluctuations in the gas reservoir. Such models are commonly referred to as 'equilibrium' (Finlator & Davé 2008; Davé, Finlator & Oppenheimer 2012), 'gas regulator' (Lilly et al. 2013; Peng & Maiolino 2014), or 'bathtub' (Bouché et al. 2010; Dekel & Mandelker 2014) models. Finlator & Davé (2008) crucially pointed out that simulations predict that the rate of change of the gas reservoir is small compared to the other terms, and setting this term exactly to zero results in simplifications that make the model more intuitive and insightful, while still being a realistic description of galaxy growth averaged over cosmological time-scales. We call this assumption of a non-evolving gas reservoir the 'equilibrium assumption', from which the equilibrium model follows (Davé et al. 2012). Notably, the gas regulator model does not make this assumption. Regardless, this simple framework is able to capture the essential baryon cycling processes analytically, thereby enabling a more intuitive view of how galaxy growth proceeds.

The next step in such models was to constrain the free parameters associated with baryon cycling. In Mitra, Davé & Finlator (2015, hereafter Paper I), we parametrized the equilibrium model with three variables corresponding to ejective feedback via a mass loading factor (η), preventive feedback via an evolving halo mass scale for quenching (ζ), and wind recycling via a typical recycling time for ejected material to re-accrete ($t_{\rm rec}$). For each variable, we postulated simple dependences on halo mass and redshift, along with an overall amplitude, resulting in nine free parameters. We found that our null hypothesis of a halo mass quenching scale of $\approx 10^{12}\,{\rm M}_{\odot}$ at $z = 0$ was preferred by the Bayesian evidence, which reduced our number of free parameters by one. With these eight free parameters, we then fit to observations of the stellar mass–halo mass relation, the MS, and the mass–metallicity relation from $z = 0$ to 2, using a Markov Chain Monte Carlo (MCMC) algorithm. We obtained a best-fitting reduced $\chi^2 = 1.6$ to all the data at all those epochs, which is significantly better than that is typically obtained in simulations or semi-analytic models (Somerville & Davé 2015). This demonstrates that the baryon cycling framework in the equilibrium model can provide a good description of galaxy growth, and moreover provides meaningful constraints on the baryon cycling variables themselves.

Our equilibrium model results suggest that one can fit the mean galaxy scaling relations and their cosmological evolution without explicitly including mergers. None the less, mergers add stochasticity to galaxy evolution that was not accounted for in the Mitra et al. (2015) model. In that sense, Paper I reflects a *first-order* model for galaxy evolution which only accounts for the mean evolution of the scaling relations. Meanwhile, the scatter around the mean scaling relations is driven by other processes such as environment and the fluctuations in the inflow rate owing to mergers (Davé, Oppenheimer & Finlator 2011; Goerdt et al. 2015; Mitra, Davé & Finlator 2015). Such processes thus can be regarded as yielding *second-order* deviations from the mean relations.

In this paper, we provide a quantitative test of the earlier first-order equilibrium model by investigating the variations around mean trends in the MS. Our basic aim is to show how the inflow fluctuations, predicted from a merger-tree-based approach, can give rise to observed scatter in the MS. Other groups have likewise investigated this (Dutton, van den Bosch & Dekel 2010; Forbes et al. 2014; Sparre et al. 2015b; Rodríguez-Puebla et al. 2016), generally finding 0.1–0.4 dex scatter in the stellar mass range 10^9–$10^{11}\,{\rm M}_{\odot}$, but have not done so within an MCMC-constrained equilibrium model-type framework as we do here.

This paper is structured as follows. In Section 2, we review the key features of our basic equilibrium model along with the modifications made for the purpose of this work, and present the (minor) updates to the parameter constraints including inflow fluctuations. We then present the resulting scatter in MS obtained from our model and compare it with the present observations in Section 3. Finally, we summarize and conclude our main findings in Section 4.

2 MODEL DESCRIPTION

2.1 First-order model

We begin by summarizing the main features of the basic equilibrium model, built on a simple set of equations which well approximate galaxy evolution in full hydrodynamic simulations (Finlator & Davé 2008). Unlike semi-analytical models (SAMs), these models are neither based on halo merger trees, nor do they attempt to track the formation of a disc and subsequent mergers, as in traditional galaxy formation theory (White & Frenk 1991; Mo, Mao & White 1998). Instead, we rely on the view that galaxies grow along a slowly evolving equilibrium between accretion, feedback, and star formation as outlined in Finlator & Davé (2008), Bouché et al. (2010), Davé et al. (2012), and Lilly et al. (2013):

$$\dot{M}_{\rm in} = \dot{M}_{\rm out} + {\rm SFR}, \tag{1}$$

where $\dot{M}_{\rm in}$ is the mass inflow rate on to the galaxy's star-forming region and $\dot{M}_{\rm out}$ is the outflow rate. This is a simple mass balance equation with an extra assumption that the net change of gas mass within the ISM is zero (i.e. the equilibrium assumption; Finlator & Davé 2008; Krumholz & Dekel 2012; Saintonge et al. 2013; Tacconi et al. 2013). From this it is possible to derive the equations for the SFR and metallicity within the ISM as (see Davé et al. 2012 and Mitra et al. 2015 for details)

$${\rm SFR} = \frac{\zeta \dot{M}_{\rm grav} + \dot{M}_{\rm recyc}}{1+\eta} \tag{2}$$

and

$$Z_{\rm ISM} = \frac{y{\rm SFR}}{\zeta \dot{M}_{\rm grav}}, \tag{3}$$

where $\dot{M}_{\rm grav}$ is the gravitational-driven inflow of dark matter haloes that is an outcome of Λ cold dark matter cosmology, y is the metal yield, and $\dot{M}_{\rm recyc}$ is the accretion rate of the material that was previously ejected in outflows. The above relations contain three unknown variables: η (the mass loading factor or the ejective feedback parameter), ζ (preventive feedback), and $t_{\rm rec}$ (wind recycling time or the recycling parameter) which are collectively known as *baryon cycling parameters* (Davé et al. 2012).

Despite ongoing efforts and improvements, the baryon cycling parameters remain difficult to constrain observationally, because

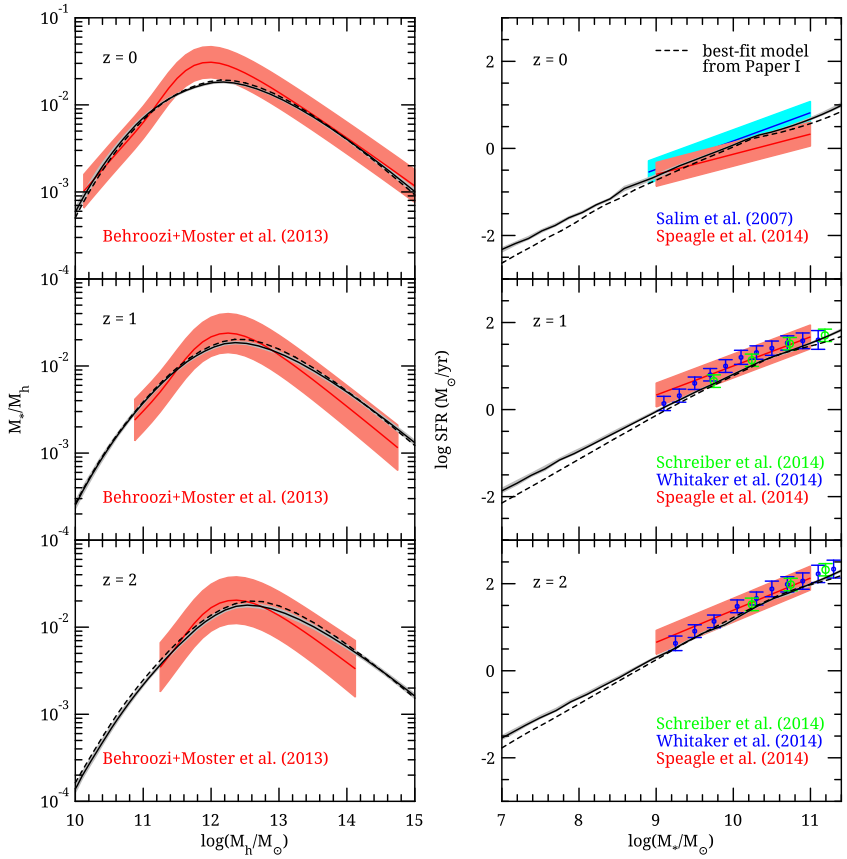

Figure 1. MCMC constraints on our first-order equilibrium model for the stellar mass–halo mass relation (left-hand panel) and the SFR–M_* relation (right-hand panel) at $z = 0$, 1, and 2. The solid black lines denote the best-fit model, whereas the thin grey shaded regions refer to their 1σ confidence limits (CLs). All the errors on observed data sets, described in Section 2.1, indicate the corresponding 1σ uncertainties. The best-fitting model from our Paper I is shown by dashed black lines for comparison.

inflows and outflows generally occur in diffuse, multiphase circumgalactic gas, which is challenging to fully characterize via either absorption or emission probes. The equilibrium model, instead, provides a way to constrain these parameters from the global demographic evolution of the galaxy population, within the context of the baryon cycling paradigm. To do so, we represent them by eight free variables that quantify their behaviour with halo masses and redshifts (Mitra et al. 2015):

$$\eta = \left(\frac{M_{\rm h}}{10^{\eta_1+\eta_2\sqrt{z}}}\right)^{\eta_3}, \tag{4}$$

$$t_{\rm rec} = \tau_1 \times 10^9 {\rm yr} \times (1+z)^{\tau_2} \left(\frac{M_{\rm h}}{10^{12}}\right)^{\tau_3}, \tag{5}$$

$$\zeta_{\rm quench} = {\rm MIN}\left[1, \left(\frac{M_{\rm h}}{M_{\rm q}}\right)^{\zeta_1}\right], \times \frac{M_{\rm q}}{10^{12}\,{\rm M}_\odot} = (0.96 + \zeta_2 z), \tag{6}$$

where $\zeta_{\rm quench}$ is the quenching feedback parameter and $M_{\rm q}$ is the quenching mass. We then employ a Bayesian MCMC approach using recent measurements of three well-known galaxy scaling relations that relate the halo mass, stellar mass, SFR, and metallicity of galaxies: (i) the stellar mass (M_*) versus halo mass ($M_{\rm h}$) relation (Behroozi, Wechsler & Conroy 2013; Moster, Naab & White 2013), (ii) the stellar mass versus gas-phase metallicity (MZR) relation (Andrews & Martini 2013; Steidel et al. 2014; Zahid et al. 2014; Sanders et al. 2015), and (iii) the stellar mass versus SFR relation (Speagle et al. 2014; Whitaker et al. 2014; Schreiber et al. 2015). To properly represent the evolution of the galaxy population, we consider these relations over a significant fraction of cosmic time, at redshifts $z = 0$ (today), 1 ($\sim$6 Gyr ago), and 2 ($\sim$10 Gyr ago). We refer the reader to Paper I for a detailed description of this analysis method. The only modification we make here is that now we compute the $\dot{M}_{\rm grav}$ from simulations in a different way (discussed later in this section), rather than what we used earlier (i.e. a simple fitting formula from Dekel et al. 2009).

We show the match between those scaling relations and our best-fitting model predictions in Fig. 1 by solid black lines, which are quite similar to what we obtained in fig. 2 of Paper I, shown in dashed lines. Note that, all the error bars here reflect 1σ or 68 per cent confidence limits (CL) around the mean. The agreement is again quite good, with an overall reduced χ^2 value of $\approx$2. The best-fitting values and 68 per cent CL for all eight parameters are listed in Table 1. The results from Paper I are also shown here for comparison, which are again comparable to what we obtain here. We use the Bayesian evidence to ensure that removing any one of these eight parameters is not statistically favoured. Overall, neither hydrodynamic simulations nor SAMs employing many more parameters are able to achieve such a good match across such a wide range of redshifts. Note that up till now, we have not explicitly considered the scatter around the scaling relations, and instead we only aim to fit the mean trends. As such, we refer to this as the *first-order* equilibrium model for galaxy evolution. In the following section, we shall see

Table 1. MCMC results from the first-order model: best-fitting values and 68 per cent CL on the all eight parameters for this paper and our Paper I.

Parameters	Best-fitting value and 1σ errors (This paper)	(Paper I)
η_1	$10.85^{+0.06}_{-0.06}$	$10.98^{+0.07}_{-0.10}$
η_2	$0.81^{+0.07}_{-0.07}$	$0.62^{+0.07}_{-0.06}$
η_3	$-1.15^{+0.08}_{-0.07}$	$-1.16^{+0.06}_{-0.06}$
τ_1	$1.12^{+0.37}_{-0.24}$	$0.52^{+0.24}_{-0.07}$
τ_2	$-0.62^{+0.11}_{-0.21}$	$-0.32^{+0.06}_{-0.20}$
τ_3	$-0.47^{+0.05}_{-0.06}$	$-0.45^{+0.10}_{-0.07}$
ζ_1	$-0.45^{+0.07}_{-0.07}$	$-0.49^{+0.07}_{-0.08}$
ζ_2	$0.51^{+0.15}_{-0.17}$	$0.48^{+0.13}_{-0.12}$

how one can get a reasonable scatter in M_*–SFR relation from the fluctuations of inflow rates using a simple probabilistic approach.

2.2 New features

We now discuss the additional features of our model which we have implemented in this work to generate the scatter in halo accretion rate. To do so, we now need to consider the fact that the accretion of material into haloes is not smooth, but rather arrives in lumps. For the dark matter, this corresponds to halo merging, which we can express using an analytical fitting formula for the dimensionless mean merger rate, $\mathrm{d}N_\mathrm{m}/\mathrm{d}\,\epsilon\,\mathrm{d}z$, where ϵ is the merger mass ratio $M_\mathrm{subhalo}/M_\mathrm{parent}$ (Fakhouri, Ma & Boylan-Kolchin 2010):

$$\frac{\mathrm{d}N_\mathrm{m}}{\mathrm{d}\epsilon \mathrm{d}z}(M,\epsilon,z) = A\left(\frac{M}{10^{12}\,\mathrm{M}_\odot}\right)^{\alpha}\epsilon^{\beta}\exp\left(\frac{\epsilon}{\bar{\epsilon}}\right)^{\gamma}(1+z)^{\eta}. \quad (7)$$

The free parameters A, $\bar{\epsilon}$, α, β, γ, and η are obtained by fitting to an N-body simulation based on Millennium (Springel et al. 2005) and Millennium-II (Boylan-Kolchin et al. 2009) simulations, but with a cosmology consistent with Planck Collaboration XIII (2016). The best-fitting values are $(A, \bar{\epsilon}, \alpha, \beta, \gamma, \eta) = (0.0104, 0.009\,72, 0.133, -1.995, 0.263, 0.0993)$.

The cumulative number of mergers received by a halo of mass M, of objects with mass between $M\epsilon_\mathrm{min}$ and $M\epsilon_\mathrm{max}$, and between redshift z_0 and z, is then given by

$$N_\mathrm{m} = \int_{z_0}^{z}\mathrm{d}z\int_{\epsilon_\mathrm{min}}^{\epsilon_\mathrm{max}}\mathrm{d}\epsilon\,\frac{\mathrm{d}N_m}{\mathrm{d}\,\epsilon\,\mathrm{d}z}(M,\epsilon,z) \quad (8)$$

and

$$\frac{\mathrm{d}M}{\mathrm{d}z} = \int_{\epsilon_\mathrm{min}}^{\epsilon_\mathrm{max}} M\epsilon\,\mathrm{d}\epsilon\,\frac{\mathrm{d}N_\mathrm{m}}{\mathrm{d}\epsilon}(M,\epsilon,z), \quad (9)$$

from which the mass accretion rate $\dot{M}_\mathrm{h}$ can be calculated by a transformation of variables from redshift z to time t. This allows us to compute the baryonic inflow rate as $\dot{M}_\mathrm{grav} = f_\mathrm{b}\dot{M}_\mathrm{h}$. We choose $\epsilon_\mathrm{min} = 10^4\,\mathrm{M}_\odot/M_\mathrm{parent}$, thereby capturing all mergers down to $M_\mathrm{h} = 10^4\,\mathrm{M}_\odot$. We have tested our model with different limits of ϵ_min, and although the 'smooth' component (discussed below) changes a bit, the overall results remain the same.

For a halo of mass M, we compute the number of mergers received in some time interval $\mathrm{d}t$ in bins of mass ratio ϵ using equation (8). We then sample the distribution of N_m as a function of ϵ to obtain the masses of individual haloes that merge with a given halo of mass M. Each such sampling produces a discrete set of masses of haloes that merge with a given parent halo of mass M. In details, we split the merger ratio integral of equation (8) into two components: (i) *merger component* – first we compute the probability (P_i) of a merger in some mass bins by summing up the integrand of equation (8). If $P_i < 1$, we generate a uniform random number between 0 and 1 and accept each merger with that probability only when P_i is greater than that random number. We stop this calculation once we get to the regime where the probability is greater than 1; (ii) *smooth component* – we do the normal integration down to ϵ_min from the point where we stopped the previous calculation. Finally, adding up both components will give the total $\dot{M}_\mathrm{h}$. We follow the same procedure for many different realizations and obtain an array of different accretion rates for a given M. In this manner, we obtain the inflow rate including fluctuations owing to halo mergers.

We have implemented this into the equilibrium model and performed an MCMC fit the mean scaling relations as was performed in Paper I. This results in the fits previously shown in Fig. 1, with the parameter constraints listed in Table 1. The fits are very similar to those arising from the first-order model.

3 RESULTS AND DISCUSSION

We now turn our attention to the main aim of this paper, namely to understand the origin of the scatter in the star-forming MS. We will assume that the fluctuations in the halo accretion rate are reflected directly in fluctuations in the SFR, as per equation (2). While it clearly takes some time for the halo inflow to reach the galaxy and form stars, we assume that once equilibrium is reached, the statistical variations are the same. To examine this in more detail, we begin by quantifying the fluctuations in $\dot{M}_\mathrm{h}$.

3.1 Halo inflow rate fluctuations

Fig. 2 displays the *total* variations in the accretion rate ($\dot{M}_\mathrm{h}$) as a function of halo mass at $z = 0$ (left-hand panel) and $z = 2$ (right-hand panel). At a fixed halo mass, we get a range of accretion rates, denoted by grey points, owing to our random selection approach over 1000 trials. The average accretion rate in bins of M_h is denoted by the solid black line, which can be compared to the red line that is the smooth halo mass accretion rate we used in Paper I. On average, the halo accretion rate is well represented by sampling the stochastic distribution.

For $z = 2$, the black curve is a very close match to the first-order mean inflow rate, as most of growth is predominantly in the 'smooth' mode (i.e. probability $P_i \gtrsim 1$). Towards lower redshifts, the merger contribution from stochasticity becomes more significant, which is consistent with trends seen from hydrodynamic simulations (e.g. Kereš et al. 2005). The *median* of the population is shown here by the solid cyan line which lies towards the denser ends of $\dot{M}_\mathrm{h}$-distribution as this quantity is less affected by extreme outliers than the mean.[1]

Here we are interested in the scatter about this mean relation. The scatter appears to be fairly asymmetric, with a large tail to higher accretion rate owing to high mass ratio mergers. A more quantitative estimate of the scatter can be obtained by fitting a

[1] The reason for choosing mean over the median in our MCMC analysis is that the former quantity is more easy (and faster) to calculate. Also the mean (black curve) closely matches the smooth halo accretion rates from the simulation (without random selection, red curves), whereas median underestimates those. So these extreme outliers are also significant to capture the whole picture.

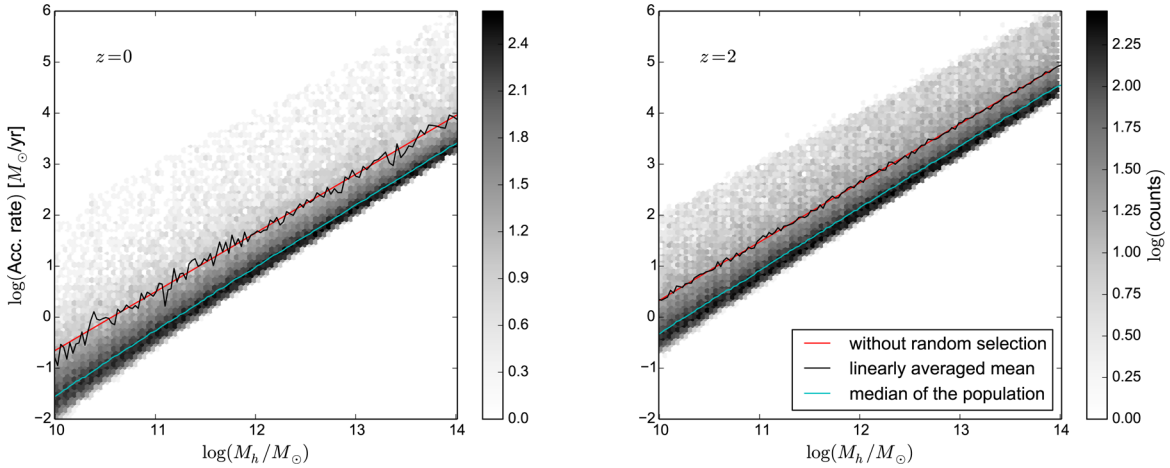

Figure 2. *Total* fluctuations in halo mass accretion rates at redshifts $z = 0$ and 2 for 1000 different realizations. The black and cyan curves represent, respectively, the linearly averaged mean and median of that distribution, whereas the red one denotes the accretion rates of the first-order model.

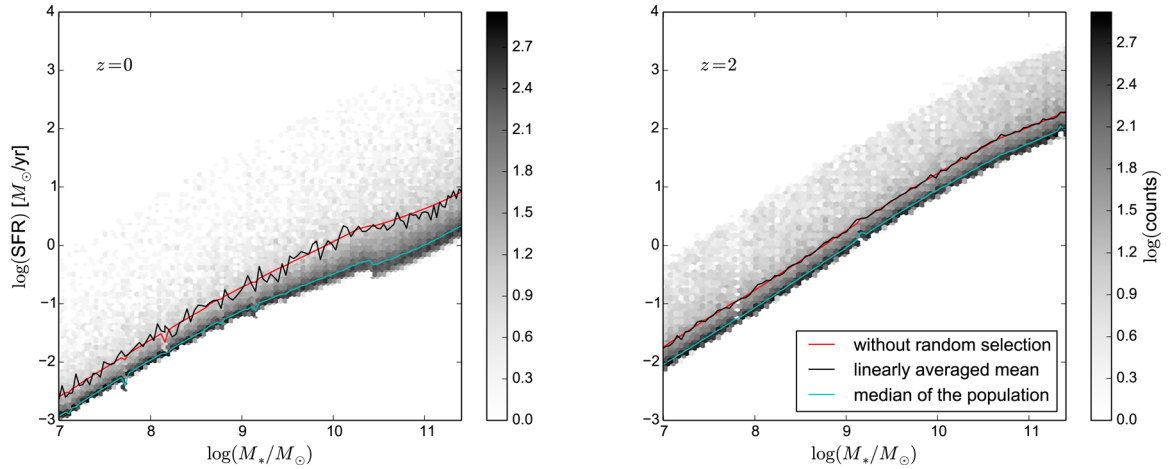

Figure 3. Same as Fig. 2, but for the M_*–SFR relation.

Gaussian or a double-Gaussian (Goerdt et al. 2015) to the histogram of that distribution; we will investigate this in the following section. We find that, although our resulting distribution of inflow rate seems skewed with a large tail, a single Gaussian fit turns out to be sufficient for our current purposes. The tail of the distribution corresponds to starbursts, which we will quantify later.

3.2 The scatter around the main sequence

To investigate how the scatter in M_*–SFR relation arises from stochasticity in the accretion rate, recall equation (2) which directly relates the SFRs to the halo mass accretion rates ($\dot{M}_{\rm grav}$). For this paper, we only investigate the scatter associated with halo inflow. It is also possible that there is scatter associated with some of the baryon cycling parameters; for instance, the mass loading factor and preventive feedback may vary between galaxies at a fixed mass (Forbes et al. 2014). For simplicity, we do not consider these additional sources of scatter in our current analysis, rather we restrict ourselves to determine the MS scatter arising only from the dispersion in inflow rates. We further note that we are intrinsically making the assumption that inflow into the halo is instantaneously reflected in inflow into the ISM; this is of course not true, but modulo a delay related to the infall time through the halo, the spectrum of halo inflow fluctuations should generally reflect the ISM inflow fluctuations. Finally, here we have estimated the SFR averaged over dt = 100 Myr, denoted SFR(100); we will consider other time-scales in Section 3.6.

The *total* variation of the star-forming MS is shown in Fig. 3. Again the linearly averaged mean agrees with the first-order model, as expected, due to large number of samples. The evolution of MS shows a shallower slope at high stellar masses at later epoch as an outcome of the slowly decreasing quenching mass in our model (Gabor & Davé 2015; Mitra et al. 2015). This behaviour is noted in observations as well (Whitaker et al. 2014).

Additionally, we have also plotted some example star formation histories, specific star formation rate sSFR(z), showing the total scatter at $M_* = 5 \times 10^9$ M$_\odot$ in Fig. 4. The sSFR(z) is seen to be evolving strongly with redshifts following sSFR $\propto (1+z)^b$, which is again consistent with the observations (Whitaker et al. 2014; Johnston et al. 2015). Unsurprisingly, the linearly averaged mean (black curves) is found to be 'bumpy' at lower z and then starts to become smooth and matches the red one at higher redshifts $z \gtrsim 2$. The observed data points shown here are from Speagle et al. (2014), Whitaker et al. (2014), and Kurczynski et al. (2016). Note that our model seems to underpredict the sSFR slightly at $z \approx 1$–2, which

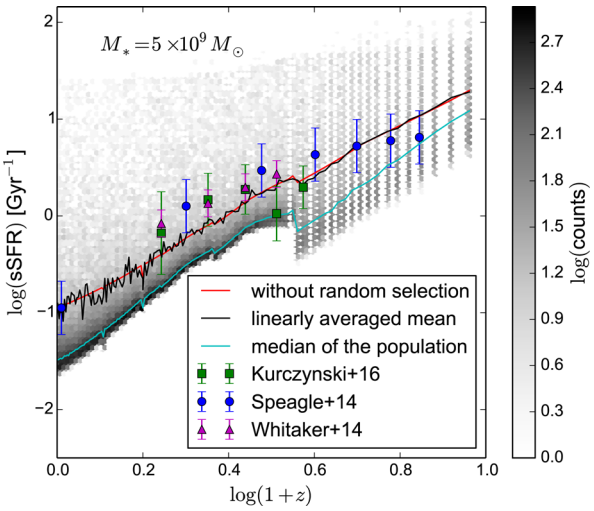

Figure 4. *Total* fluctuations in specific star formation rate (sSFR) as a function of redshift at $M_* = 5 \times 10^9$ M$_\odot$. The absence of the lumpiness in linearly averaged mean curves (black) at earlier epoch corresponds to the halo growth in 'smooth' mode.

was also seen in Fig. 1, but overall is in good agreement with the data within their observational uncertainties.

To get an estimated scatter in MS, one must fit the probability distribution function (PDF) of the SFR at some stellar mass and redshift. We have obtained the number density distribution of galaxies in six stellar mass bins spanning from 10^8 to 10^{11} M$_\odot$ as a function of their SFRs at a redshift range of $0.5 \leq z \leq 4$. We fit Gaussians to these distributions to objectively identify the MS and its outliers, similar to the analysis done by Rodighiero et al. (2011) (see also Sargent et al. 2012 for a double-Gaussian fit).

Fig. 5 shows some typical distributions at redshift ranges $0.5 < z < 1$ and $1.5 < z < 2$, where we plotted the normalized PDFs of the logarithmic SFR for mass bins $9.5 < \log(M_*/\mathrm{M}_\odot) < 10$ (left-hand panels) and $10 < \log(M_*/\mathrm{M}_\odot) < 10.5$ (right-hand panels). The Gaussian fits with the standard deviations $\sigma \approx 0.2$ dex are displayed by the solid red curve. This log–normal fit in SFR is quite good over the bulk of the curve, but there is clearly an excess at high SFR; we will return to this in Section 3.5.

3.3 Comparison to previous observations and models

A key aim of this paper is to determine whether the simple equilibrium model can account for the observed scatter in the MS based on fluctuations in the inflow rate. To this end, we now compare our scatter predictions, along with their trends with galaxy mass and redshift, versus a range of recent observations. We also discuss comparisons to recent models and simulations that have predicted the MS scatter.

Fig. 6 shows the estimated intrinsic scatters on the MS for all six stellar mass bins at various redshifts, computed as the width in dex of the log-normal fit. The individual values are presented in Table 2. Overall, we find that the standard deviation

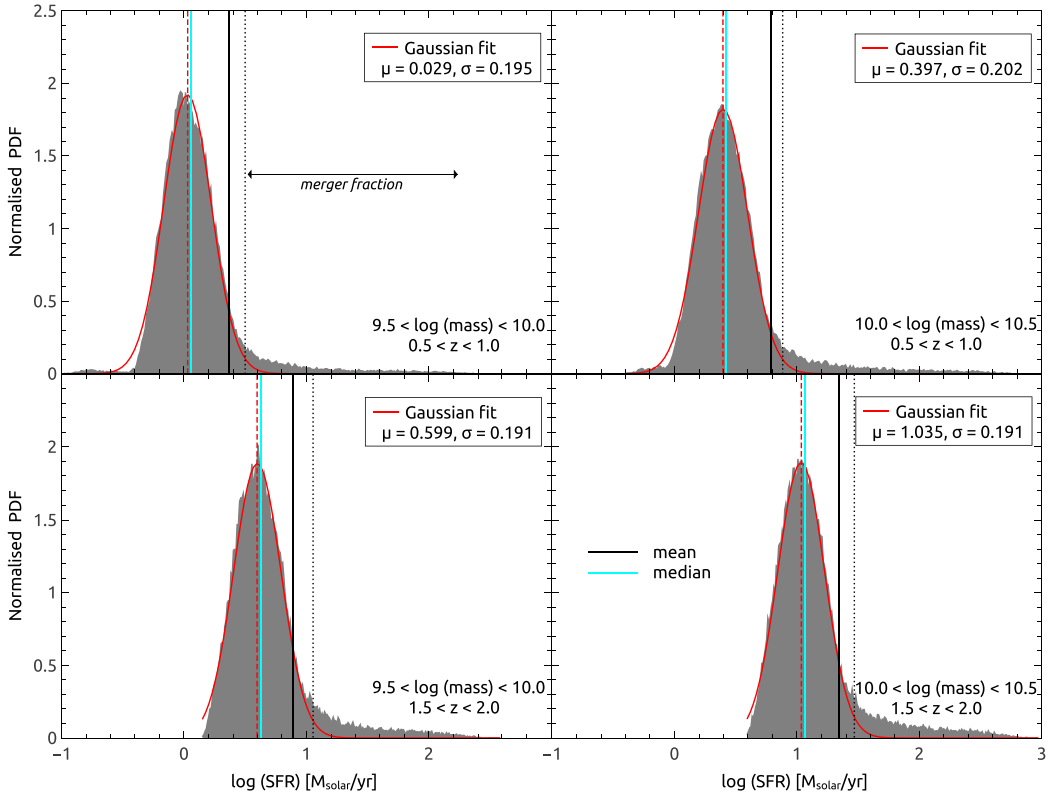

Figure 5. Normalized distributions (filled grey histograms) of SFRs in selected mass–redshift bins quoted in the figure. Shown in filled red curves are the individual Gaussian fits with a dispersion of ∼0.2 dex to that distribution. Deviations (dotted black vertical lines) from the Gaussian are seen at ∼0.45–0.5 dex (or 2.4σ) above the mean of the fits (dashed red vertical lines). The mean and median of those distributions are also shown here by solid black and cyan vertical lines, respectively. Medians are found to be less affected by the extreme outliers at higher SFR ends and closely match the mode of the distributions, as expected.

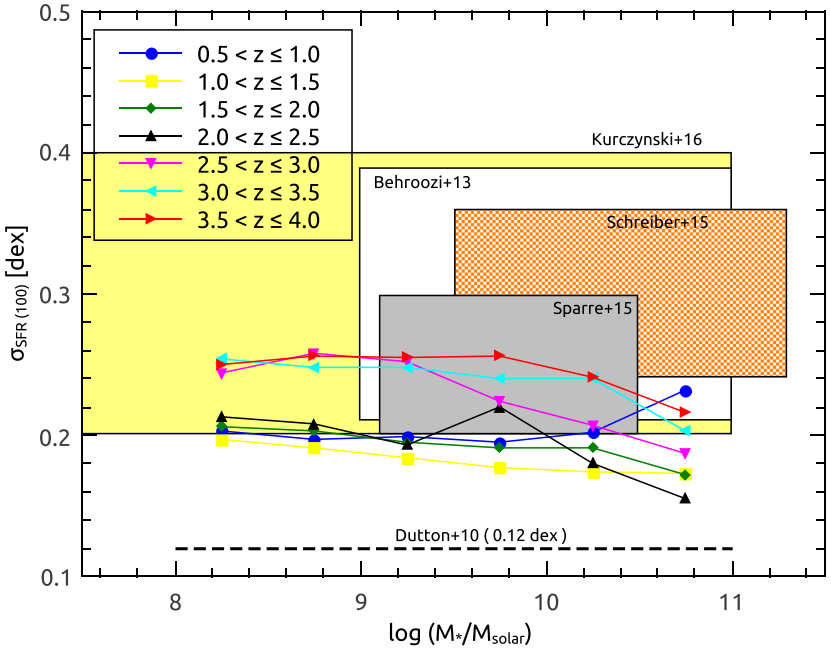

Figure 6. The MS scatter (1σ) at the redshift range $0.5 \leq z \leq 4$. In all cases, we estimate the SFR averaged over 100 Myr. For comparison, we show the typical scatter obtained from observations by Schreiber et al. (2015) (shaded orange bands) and Kurczynski et al. (2016) (shaded yellow; intrinsic scatter of 0.2–0.4 dex). For models, we show the Illustris simulation results (Sparre et al. 2015b) and results from the abundance matching models of Behroozi et al. (2013, see their table 9) by the shaded grey and empty middle bands, respectively. The prediction from the analytic disc model of Dutton et al. (2010) is shown as the dashed black line.

Table 2. Intrinsic scatter around the MS of galaxies in bins of different stellar masses and redshifts averaged over time-scale 100 Myr (30 Myr). Typically, the scatter increases when we decrease the time-scale. Overall, the 1σ dispersion of ∼0.2–0.25 dex for the 100 Myr case (or ∼0.2–0.3 dex for 30 Myr) is broadly comparable with various recent observations.

Redshift range	$\sigma_{\rm SFR(100)}$ [$\sigma_{\rm SFR(30)}$] in dex					
	$8 < \log M_* < 8.5$	$8.5 < \log M_* < 9$	$9 < \log M_* < 9.5$	$9.5 < \log M_* < 10$	$10 < \log M_* < 10.5$	$10.5 < \log M_* < 11$
$0.5 \leq z \leq 1$	0.203 [0.205]	0.197 [0.202]	0.199 [0.193]	0.195 [0.199]	0.202 [0.199]	0.232 [0.266]
$1 < z \leq 1.5$	0.197 [0.216]	0.191 [0.218]	0.184 [0.223]	0.177 [0.211]	0.174 [0.204]	0.173 [0.201]
$1.5 < z \leq 2$	0.206 [0.226]	0.203 [0.222]	0.195 [0.216]	0.191 [0.225]	0.191 [0.227]	0.172 [0.207]
$2 < z \leq 2.5$	0.213 [0.290]	0.208 [0.277]	0.193 [0.289]	0.220 [0.220]	0.180 [0.210]	0.155 [0.186]
$2.5 < z \leq 3$	0.244 [0.251]	0.258 [0.296]	0.252 [0.294]	0.224 [0.305]	0.207 [0.311]	0.187 [0.275]
$3 < z \leq 3.5$	0.254 [0.313]	0.248 [0.305]	0.248 [0.307]	0.240 [0.304]	0.240 [0.301]	0.203 [0.282]
$3.5 < z \leq 4$	0.250 [0.285]	0.256 [0.317]	0.255 [0.308]	0.256 [0.298]	0.241 [0.285]	0.216 [0.296]

$\sigma_{\rm SFR(100)}$ is ∼0.2–0.25 dex, showing no significant trend with redshifts or stellar mass, except for a weak overall increase at higher redshifts.

Using the *Spitzer* MIPS observations, Noeske et al. (2007) and Elbaz et al. (2007) obtained a 0.3 dex scatter (1σ) around the MS at $z \sim 1$, while Whitaker et al. (2012) reported a dispersion of 0.34 dex in the range $0 < z < 2.5$ using a sample of galaxies selected from the NEWFIRM Medium-Band Survey. Similarly, Rodighiero et al. (2011) determined a value of 0.24 dex scatter using mostly ultraviolet (UV)-derived SFRs. Recently, using the deep UV to NIR observations in the CANDELS fields, Schreiber et al. (2015) reported a scatter around the average SFR to be ∼0.3 dex. These observational results refer to the total scatter, which includes observational measurement uncertainties. Several groups have attempted to correct for measurement errors to determine the intrinsic scatter. Guo, Zheng & Fu (2013) found intrinsic sSFR dispersions of 0.18–0.31 dex in the stellar mass range of $9.5 < \log(M_*/{\rm M}_\odot) < 11.5$ at $z \sim 0.7$, while Kurczynski et al. (2016) found an intrinsic scatter of 0.2–0.4 dex in the redshift range $0.5 < z < 3$ and in the mass range $7 < \log(M_*/{\rm M}_\odot) < 11$. Using the MOSDEF Survey of SFGs with Hα and Hβ spectroscopy, Shivaei et al. (2015) studied the MS relation at $z \sim 2$ and found an intrinsic scatter of ∼0.31 dex for the SFR(Hα) sample, which is 0.05 dex larger than what they measured from UV SFRs. Speagle et al. (2014) combined various measurements of the star-forming MS from literature by recalibrating them to use a common set of assumptions. After accounting for intrinsic scatter among SFR indicators, they found that the 'true intrinsic' scatter is actually ∼0.2 dex rather than the often reported 0.3 dex value and it remains roughly constant over cosmic time. Generally, observations tend to suggest a total scatter of 0.3–0.4 dex depending on mass and redshift, with the intrinsic scatter being as low as 0.2 dex.

The scatter we predict from the equilibrium model is overall in very good agreement with these observations. The model yields an intrinsic scatter of ∼0.2 dex, with only a very slight mass dependence increasing to lower masses. We also do not find a strong redshift dependence out to $z \sim 2$, though it increases at all masses at $z \gtrsim 2.5$.

There are indications, particularly from Kurczynski et al. (2016), that the intrinsic scatter may be significantly higher than 0.2 dex in some cases. Remember that our current approach only includes scatter associated with inflow fluctuations, while, in principle, there could be intrinsic variations in the mass outflow rate (η) or in preventive feedback (ζ), which would give extra scatter to the overall $\sigma_{\rm SFR}$. None the less, it is interesting that the lowest measured intrinsic scatters are quite consistent with our prediction just from inflow fluctuations. This limits the stochasticity in outflows to relatively modest values, and suggests that galactic outflows must be a fairly steady phenomenon at least when averaged over ∼100 Myr. Alternatively, there may be some relationship between outflow rates and inflow stochasticity such that a relatively tight correlation is maintained owing to correlated scatter.

Numerous galaxy evolution simulations and semi-analytical or analytical models have likewise made predictions for the intrinsic scatter around the M_*–SFR relation. Sparre et al. (2015b) used the Illustris simulation to obtain a ∼0.2–0.25 dex scatter for $M_* \lesssim 10^{10.5}\,{\rm M}_\odot$, while the semi-analytic model for disc galaxy evolution by Dutton et al. (2010) predicted a lower scatter of 0.12 dex in SFR. Note that, this value is much less than the observed one as the latter is likely to be dominated by observational uncertainties. However, this might also reflect the fact that Dutton et al. (2010) underestimated the true scatter due to their simplified treatment of the halo mass accretion history and thus additional sources of intrinsic scatter are probably required in their model. Using zoom-in hydrocosmological simulations of massive galaxies at $z > 1$, Tacchella et al. (2016) examined the evolution of SFGs across the MS through gas *compaction*, *depletion*, and *replenishment* and measured a *true* scatter of ∼0.27 dex with a slightly increasing trend towards lower redshifts. Note that, if these processes are independent of inflow fluctuations, then these would contribute additional scatter around the MS. Recently, Rodríguez-Puebla et al. (2016) have reported the σ to be ∼0.35–0.45 dex from a simple analytical approach based on the crucial assumption that the stellar-to-halo mass ratio is nearly independent of redshift up to $z \sim 4$. In general, our numbers are similar to that obtained from Illustris, which supports the notion that MS fluctuations in hydrodynamic simulations are arising from inflow stochasticity. The analytic models, on the other hand, have more widely varying predictions; this may owe to the fact that some of their assumptions may not be reflective of how galaxy formation proceeds via baryon cycle-driven growth.

Our method is quite similar in many ways to that in Forbes et al. (2014), who examine the scatter in the MS as well as in the MZR and FMR arising from the scatter in dark matter accretion rates as well as some of the baryon cycling parameters from their bathtub model. Considering a typical *N*-body predicted stochastic scatter in the accretion rates, they found that the scatter in both the MS and MZR at fixed stellar mass is comparable to, or larger than, the observed ones and roughly independent of halo mass and redshift. Although we compute stochasticity in a different way and use a full MCMC approach to characterize the best-fitting relations, we echo their general conclusion that fluctuations in feedback parameters must be sub-dominant.

3.4 Mass and redshift dependence of the scatter

The mass and redshift dependence of the MS scatter has also been a subject of some debate. Cosmological models like Illustris generally predict a constant scatter to low masses (Sparre et al. 2015b), although this simulation predicts a growing scatter at high masses as quenched galaxies enter into their sample. In contrast, the FIRE simulations analysed by Sparre et al. (2015a) find that $M_* \sim 10^9\,{\rm M}_\odot$ galaxies can have extremely bursty SFHs, with a scatter well over 0.5 dex on short time-scales, and argued this owed to their high resolution and more self-consistent implementation of feedback processes.

Observations are also starting to characterize the mass dependence of the MS scatter. Results from Rodighiero et al. (2011), Whitaker et al. (2012), and Schreiber et al. (2015), generally found the scatter to be independent of M_*, and also z, down to M_* as low as $\sim 10^{9.5}\,{\rm M}_\odot$ at various epochs. Also, Rodríguez-Puebla et al. (2016) did not notice a clear trend with mass to even lower masses.

In the equilibrium model, the scatter arises purely from halo inflow fluctuations. Since halo mass growth rates are fairly self-similar, one does not expect a strong trend with halo mass, and thus stellar mass, in the scatter. Hence, it is expected that our scatter has only a very weak mass dependence, which is what we see in Fig. 6. This seems to be broadly in agreement with observations, which again supports the notion that SFR fluctuations are primarily driven by inflow fluctuations. In the case of FIRE, the larger scatter is likely driven by the strong variations in outflow strength on small time-scales in dwarf galaxies; as observations of such galaxies improve, this will provide a significant constraint how bursty low-mass galaxy SFHs can be.

We also find no redshift dependence in the scatter up to $z \sim 2$, and then a modest increase at higher redshifts. This is in agreement with the observations by Kurczynski et al. (2016) who also found essentially no evolution in intrinsic scatter, with a typical value of $\sigma \sim 0.25$ from $z \sim 1$ to 3. They did find a higher scatter at $z \lesssim 1$, which likely owes to the inclusion of galaxies on their way to being quenched. Meanwhile, our results are in agreement with the model by Rodríguez-Puebla et al. (2016) who averaged the halo accretion rate over the dynamical time-scale and found no redshift dependence. Overall, the predicted lack of a strong redshift dependence seems consistent with available data.

In summary, the equilibrium model predicts the SFR scatter at a given M_* that is comparable to the lowest values for the observed intrinsic scatter, and is generally below the observed values for the total scatter. Models show a larger range in scatter depending on assumptions and techniques, but predictions of the equilibrium model generally agree most closely with predictions taken directly from cosmological hydrodynamic simulations. We do not find a strong mass or redshift dependence in the scatter, suggesting that dwarf/early galaxy SFHs are not expected to be significantly burstier. This is generally in agreement with the available data, and bolsters our claim that halo inflow fluctuations, which are expected to be fairly self-similar with mass, drive SFR fluctuations.

3.5 Merger-driven starbursts

Not all galaxies lie within the scatter of the MS. Galaxies fall below the MS as they are quenched by a variety of processes such as black hole feedback or gas stripping processes (Somerville & Davé 2015). The outliers above the MS are starburst galaxies, and can be identified in our model as high upwards fluctuations in the inflow rate. Even though the equilibrium model does not account for internal dynamical processes that can drive the most extreme starbursts (Mihos & Hernquist 1996; Sanders & Mirabel 1996), such galaxies are very rare and require special initial conditions, while more typical mergers are far less extreme (Cox et al. 2008). We can thus quantify in our model the fraction of galaxies in such mergers, as well as their global contribution to overall star formation.

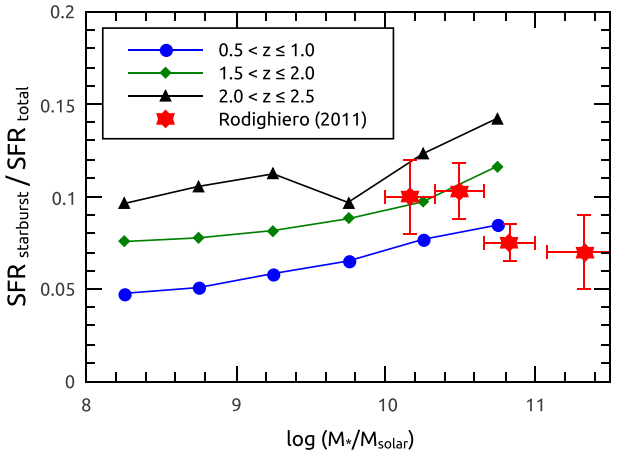

Figure 7. Contribution of starburst galaxies (2.4σ above the MS) to the total SFR as a function of stellar mass at different redshift bins. The observed Rodighiero et al. (2011) data sets (red points with error bars) at $1.5 < z < 2.5$ are also plotted for comparison.

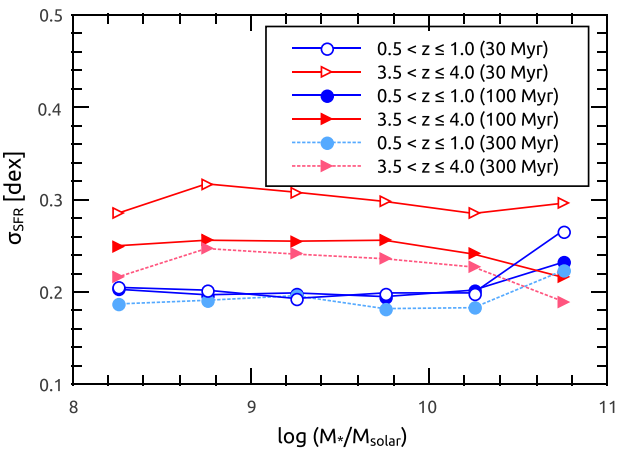

Figure 8. Scatter in MS with the SFR averaged over different time-scales (30, 100, and 300 Myr). Overall, the dispersion increases for shorter time-scale variability and declines for longer time-scales.

We quantify the merger-induced fraction of SFR by computing the excess SFR owing to mergers from each histogram in Fig. 7. To compare with data, we adopt a cut-off of ∼0.45–0.5 dex (or 2.4σ) above the MS (vertical dotted line), and declare the fraction of SFR occurring above this to be merger induced; this is analogous to the procedure performed in observations by Rodighiero et al. (2011). The resulting values are very similar to that obtained by directly summing the difference between the histograms and the best-fitting Gaussians in Fig. 5.

Fig. 7 shows that the amount of merger-induced SF is generally quite small, around ∼5–15 per cent, at all epochs out to $z \sim 2.5$. There is a mild trend for an increase in merger-induced SF towards higher redshifts. Since these galaxies are contributing disproportionately to the SFR relative to their numbers, the fraction of galaxies that lie in this merger regime is even smaller.

Our predicted values are quite consistent with the observational determination by Rodighiero et al. (2011), at the relevant redshift $z \sim 2$. Also we do not predict a strong mass dependence, which is also generally consistent with these data. Interestingly, we predict a weak increase in merger-induced SF to higher masses, which is expected because halo mergers are increasingly important at high halo masses (Guo & White 2008). The data if anything seem to favour an anticorrelation with mass, but the dynamic range is not yet large enough to make conclusive statements. There are, however, some observational indications of bursty star formation at lower masses on time-scales much less than ∼100 Myr (Weisz et al. 2012; Kauffmann 2014; Guo et al. 2016). Even though these bursty population of low-mass galaxies can contribute as much as 50–60 per cent to their present-day mass (Kauffmann 2014), the equilibrium model does not predict any such trend.

Overall, during the peak activity of cosmic star formation until today, galaxy growth in our equilibrium model is strongly dominated by galaxies lying within the Gaussian scatter around the MS. This conclusion is consistent with currently available observations, as well as long-standing predictions from cosmological simulations (Murali et al. 2002; Kereš et al. 2005). This motivates the idea that merger-induced star formation represents a second-order effect in global galaxy growth, while the primary driver remains steady (but mildly fluctuating) gravitational inflow.

3.6 Time-scale variability in SFRs

So far, we have estimated the dispersion in MS using the SFRs averaged over 100 Myr. However, the inferred SFRs of galaxies are sensitive to the choice of time-scale over which the SFR is averaged (Kennicutt & Evans 2012; Hopkins et al. 2014; Sparre et al. 2015b). Hα tends to measure star formation traced by the most massive stars hence and fluctuations on scales of tens of million years, while UV-based measures tend to trace somewhat less massive (OB) stars with time-scales of ∼100 Myr. Far-infrared measures come from dust-reprocessed light which can trace even longer time-scales. Hence, it is interesting to measure the scatter in SFR smoothed over different time intervals.

Fig. 8 shows the SFR scatter averaged over 30 Myr (see also Table 2) and 300 Myr, along with our canonical value of 100 Myr, for two different redshift ranges: $0.5 < z \leq 1$ (circle) and $3.5 < z \leq 4$ (right triangle). Generally, the scatter decreases when we increase the time-scale, which is expected as the SFHs of galaxies are essentially smoothed out for longer time-scale variability. This is qualitatively in agreement with other studies (Hopkins et al. 2014; Sparre et al. 2015b).

In detail, at low redshifts the differences among time-scales are fairly negligible. This is expected because the accretion time-scales at late epochs are quite long. Meanwhile, at high redshifts there is a very clear trend, with the 30 Myr scatter being ≈0.3 dex as opposed to the longer time-scale scatter being ≈0.25 dex. Still, all these variations are rather modest. Hence, the equilibrium model does not predict that short time-scale SFR indicators as Hα will display significantly greater scatter. It remains to be seen if this is in agreement with observations.

4 SUMMARY

The equilibrium model for galaxy evolution highlights galactic inflows and outflows as the main governor of galaxy growth, in accord with the emerging baryon cycling paradigm for galaxy self-regulation. Using a Bayesian MCMC approach, we showed in Paper I that our baryon cycling-based model can match observed mean galaxy scaling relations across the majority of cosmic time better and with many fewer parameters than in traditional merger-tree-based semi-analytic models.

In this work, we test the basic equilibrium model by capturing the 'second-order' galaxy evolutionary processes, i.e. the deviations from these mean trends, which we assume here are driven by the fluctuations in the inflow rate, including mergers. The goal is to understand the origin of the scatter in the scaling relation between the stellar mass and the SFR (known as the MS), and quantify the contribution from the scatter in mean dark matter accretion rates.

We introduce a novel approach to incorporate fluctuations in the inflow rates by sampling the merger rates derived from *N*-body simulations. Assuming that such dark matter fluctuations in halo accretion are proportionally translated into baryonic inflow fluctuations into the galaxy, we make predictions for the scatter around the SFG MS. We calculate the 1σ scatter within stellar mass bins spanning from $8 < \log(M_*/\mathrm{M}_\odot) < 11$ for different redshift ranges, by fitting a Gaussian to the log of the SFR distribution (i.e. a log-normal). Although the distributions of log SFR are somewhat skewed with an excess tail towards large SFR, they can still be reasonably described by a single Gaussian fit (Rodighiero et al. 2011) that encloses the MS. The tail portion corresponds to the starburst regime. We average over several different time-scales to estimate how the scatter would change amongst different SFR indicators. In this way, we quantify the intrinsic MS scatter as a function of mass, redshift, and time-scale.

Our main findings are summarized as follows:

(i) With a sufficiently large number of realizations, we show that the linearly averaged mean of that inflow rate distribution closely follows the smooth accretion rate that we assumed in Paper I. Hence, we confirm that our stochastic approach closely reproduces the results from our first-order model in Paper I. For higher redshifts, they are almost identical as we enter a regime of smooth accretion mode, while to lower redshifts the contribution from mergers grows (though is still sub-dominant).

(ii) The merger-based inflow fluctuations translate into a significant intrinsic scatter in the star-forming MS of $\approx$0.2–0.25 dex. This is generally somewhat lower than observed values of the scatter which include measurement error, and is comparable to the lowest values when observations attempt to infer the intrinsic scatter by subtracting off measurement error. Interestingly, our reported value is in excellent agreement with the results from Speagle et al. (2014) where they compile various observed data sets and find the true scatter in MS, after correcting for the observation-induced errors, to be $\sim$0.2 dex rather than $\sim$0.3 dex. This highlights our primary result that fluctuations in the dark matter accretion rate are the primary driver of the observed MS scatter.

(iii) We predict very little dependence on stellar mass in the scatter down to $M_* = 10^9\,\mathrm{M}_\odot$. This trend is broadly in agreement with observational studies (Whitaker et al. 2012; Schreiber et al. 2015; Kurczynski et al. 2016; Rodríguez-Puebla et al. 2016). It is also generally consistent with hydrodynamic simulations, but is less consistent with the higher resolution FIRE simulations that show must burstier star formation at low masses owing to a duty cycle set up by intermittent strong feedback. If such burstiness is eventually confirmed in observations, it would suggest that we must include variability in our mass outflow rate η at low masses into our equilibrium model. Currently, however, most of the observations do not conclusively favour this (see also Weisz et al. 2012; Kauffmann 2014; Guo et al. 2016).

(iv) We predict that the MS scatter has only minimal redshift dependence, increasing slightly at high redshifts. We also show that at later epochs, the scatter is mostly independent of SFR time-scale, while at early epochs it increases modestly to shorter time-scales.

(v) The contribution to the global SFR from merger-induced star formation is minimal at all explored redshifts, typically 5–15 per cent with a mild trend towards being higher at high redshifts. Hence, starbursts are strongly sub-dominant in terms of overall stellar growth in our models. This is consistent with available observations and cosmologically situated models.

Our results indicate that we have successfully tested the equilibrium model by predicting scatter around the MS purely from inflow fluctuations, and that such fluctuations are the primary driver for deviations from the MS.

In this work, we have not considered fluctuations in the baryon cycling parameters. Potentially, one could use the scatter in the mass–metallicity relation to constrain this. In the absence of recycling, the mass dependence of the metallicity is purely set by that of η, so in principle the mass–metallicity scatter constrains the η scatter. But one could likely also introduce scatter in ζ and/or $t_{\rm rec}$ to achieve a similar result. Satellites also deviate systematically in metallicity from central galaxies, so we are engaged in developing models to incorporate satellite stripping processes in order to quantify their contribution to the MS scatter (Simha et al. in preparation). Still, given that the scatter in mass–metallicity is typically quite small ($\sim$0.1 dex), this suggests that inflow fluctuations will continue to dominate the MS scatter.

The equilibrium model is developing into a valuable and intuitive tool to study galaxy evolution within a simple baryon cycling framework. In a sense, this model is starting down the road to 'precision galaxy formation', in which the first-order parameters that establish galaxy growth can start to be constrained by observations, in analogy with the main parameters in precision cosmology. Meanwhile, other processes such as galaxy mergers represent second-order effects to global galaxy growth, and impact a different set of observables such as galaxy morphological transformations and satellite-specific processes. Incorporating halo mergers in a probabilistic fashion as we have done here is a key step towards extensions of the equilibrium model that will develop this tool into a leading platform for understanding galaxy evolution within a baryon cycling framework.

ACKNOWLEDGEMENTS

SM, RD, and VS acknowledge support from the South African Research Chairs Initiative and the South African National Research Foundation. Support for RD was also provided by NASA ATP grant NNX12AH86G to the University of Arizona.

REFERENCES

Andrews B. H., Martini P., 2013, ApJ, 765, 140
Balogh M. L., Pearce F. R., Bower R. G., Kay S. T., 2001, MNRAS, 326, 1228
Behroozi P. S., Wechsler R. H., Conroy C., 2013, ApJ, 770, 57
Bouché N. et al., 2010, ApJ, 718, 1001
Boylan-Kolchin M., Springel V., White S. D. M., Jenkins A., Lemson G., 2009, MNRAS, 398, 1150
Christensen C. R., Davé R., Governato F., Pontzen A., Brooks A., Munshi F., Quinn T., Wadsley J., 2016, ApJ, 824, 57
Cox T. J., Jonsson P., Somerville R. S., Primack J. R., Dekel A., 2008, MNRAS, 384, 386
Daddi E. et al., 2007, ApJ, 670, 156
Davé R., Oppenheimer B. D., Finlator K., 2011, MNRAS, 415, 11
Davé R., Finlator K., Oppenheimer B. D., 2012, MNRAS, 421, 98
Davé R., Thompson R., Hopkins P. F., 2016, MNRAS, 462, 3265
Dekel A., Mandelker N., 2014, MNRAS, 444, 2071
Dekel A. et al., 2009, Nature, 457, 451

Di Cintio A., Brook C. B., Macciò A. V., Stinson G. S., Knebe A., Dutton A. A., Wadsley J., 2014, MNRAS, 437, 415
Dutton A. A., van den Bosch F. C., Dekel A., 2010, MNRAS, 405, 1690
Elbaz D. et al., 2007, A&A, 468, 33
Fakhouri O., Ma C.-P., Boylan-Kolchin M., 2010, MNRAS, 406, 2267
Finlator K., Davé R., 2008, MNRAS, 385, 2181
Forbes J. C., Krumholz M. R., Burkert A., Dekel A., 2014, MNRAS, 443, 168
Gabor J. M., Davé R., 2015, MNRAS, 447, 374
Genel S. et al., 2014, MNRAS, 445, 175
Goerdt T., Ceverino D., Dekel A., Teyssier R., 2015, MNRAS, 454, 637
Guo Q., White S. D. M., 2008, MNRAS, 384, 2
Guo K., Zheng X. Z., Fu H., 2013, ApJ, 778, 23
Guo Y. et al., 2016, preprint (arXiv:1604.05314)
Henriques B. M. B., White S. D. M., Thomas P. A., Angulo R. E., Guo Q., Lemson G., Springel V., 2013, MNRAS, 431, 3373
Hopkins P. F., Kereš D., Oñorbe J., Faucher-Giguère C.-A., Quataert E., Murray N., Bullock J. S., 2014, MNRAS, 445, 581
Johnston R., Vaccari M., Jarvis M., Smith M., Giovannoli E., Häußler B., Prescott M., 2015, MNRAS, 453, 2540
Kauffmann G., 2014, MNRAS, 441, 2717
Kennicutt R. C., Evans N. J., 2012, ARA&A, 50, 531
Kereš D., Katz N., Weinberg D. H., Davé R., 2005, MNRAS, 363, 2
Krumholz M. R., Dekel A., 2012, ApJ, 753, 16
Kurczynski P. et al., 2016, ApJ, 820, L1
Lilly S. J., Carollo C. M., Pipino A., Renzini A., Peng Y., 2013, ApJ, 772, 119
Martin C. L., 2005, ApJ, 621, 227
Mihos J. C., Hernquist L., 1996, ApJ, 464, 641
Mitra S., Davé R., Finlator K., 2015, MNRAS, 452, 1184 (Paper I)
Mo H. J., Mao S., White S. D. M., 1998, MNRAS, 295, 319
Moster B. P., Naab T., White S. D. M., 2013, MNRAS, 428, 3121
Murali C., Katz N., Hernquist L., Weinberg D. H., Davé R., 2002, ApJ, 571, 1
Muratov A. L., Kereš D., Faucher-Giguère C.-A., Hopkins P. F., Quataert E., Murray N., 2015, MNRAS, 454, 2691
Noeske K. G. et al., 2007, ApJ, 660, L43
Oppenheimer B. D., Davé R., Kereš D., Fardal M., Katz N., Kollmeier J. A., Weinberg D. H., 2010, MNRAS, 406, 2325
Peng Y.-j., Maiolino R., 2014, MNRAS, 443, 3643
Planck Collaboration XIII, 2016, A&A, 594, A13
Rodighiero G. et al., 2011, ApJ, 739, L40
Rodríguez-Puebla A., Primack J. R., Behroozi P., Faber S. M., 2016, MNRAS, 455, 2592
Rubin K. H. R., Prochaska J. X., Koo D. C., Phillips A. C., Martin C. L., Winstrom L. O., 2014, ApJ, 794, 156
Saintonge A. et al., 2013, ApJ, 778, 2
Salim S. et al., 2007, ApJS, 173, 267
Sanders D. B., Mirabel I. F., 1996, ARA&A, 34, 749
Sanders R. L. et al., 2015, ApJ, 799, 138
Sargent M. T., Béthermin M., Daddi E., Elbaz D., 2012, ApJ, 747, L31
Schaye J. et al., 2015, MNRAS, 446, 521
Schreiber C. et al., 2015, A&A, 575, A74
Shivaei I. et al., 2015, ApJ, 815, 98
Somerville R. S., Davé R., 2015, ARA&A, 53, 51
Sparre M., Hayward C. C., Feldmann R., Faucher-Giguère C.-A., Muratov A. L., Kereš D., Hopkins P. F., 2015a, preprint (arXiv:1510.03869)
Sparre M. et al., 2015b, MNRAS, 447, 3548
Speagle J. S., Steinhardt C. L., Capak P. L., Silverman J. D., 2014, ApJS, 214, 15
Springel V. et al., 2005, Nature, 435, 629
Steidel C. C., Erb D. K., Shapley A. E., Pettini M., Reddy N., Bogosavljević M., Rudie G. C., Rakic O., 2010, ApJ, 717, 289
Steidel C. C. et al., 2014, ApJ, 795, 165
Tacchella S., Dekel A., Carollo C. M., Ceverino D., DeGraf C., Lapiner S., Mandelker N., Primack Joel R., 2016, MNRAS, 457, 2790
Tacconi L. J. et al., 2013, ApJ, 768, 74
Tremonti C. A. et al., 2004, ApJ, 613, 898
Weiner B. J. et al., 2009, ApJ, 692, 187
Weisz D. R. et al., 2012, ApJ, 744, 44
Wetzel A. R., Hopkins P. F., Kim J.-h., Faucher-Giguère C.-A., Kereš D., Quataert E., 2016, ApJ, 827, L23
Whitaker K. E., van Dokkum P. G., Brammer G., Franx M., 2012, ApJ, 754, L29
Whitaker K. E. et al., 2014, ApJ, 795, 104
White S. D. M., Frenk C. S., 1991, ApJ, 379, 52
Zahid H. J., Dima G. I., Kudritzki R.-P., Kewley L. J., Geller M. J., Hwang H. S., Silverman J. D., Kashino D., 2014, ApJ, 791, 130

This paper has been typeset from a TEX/LATEX file prepared by the author.